Available online at www.sciencedirect.com

SciVerse ScienceDirect

Ceramics International 38 (2012) 6311–6319

CERAMICS INTERNATIONAL

www.elsevier.com/locate/ceramint

Effect of divalent ion substitution on oxygen sensing properties of hot-spot based $Eu_{1-x}Ca_xBa_2Cu_3O_{7-\delta}$ and $Eu_{1-y}Mg_yBa_2Cu_3O_{7-\delta}$ ceramics

S.A. Yaacob, A.K. Yahya*, M.I.M. Yusof, R. Hasham

Faculty of Applied Sciences, Universiti Teknologi MARA, 40450 Shah Alam, Selangor, Malaysia

Received 16 January 2012; received in revised form 29 April 2012; accepted 30 April 2012
Available online 10 May 2012

Abstract

In this paper effects of Ca and Mg substitution on oxygen sensing properties of hot spot based Eu123 rods are reported. $Eu_{1-x}Ca_xBa_2Cu_3O_{7-\delta}$ ($x=0.2$–0.5) and $Eu_{1-y}Mg_yBa_2Cu_3O_{7-\delta}$ ($y=0.2$–0.5) ceramics were synthesized from oxide powders using the standard solid state method and fabricated into short rods. For Ca-substituted rods, after appearance of a visible hot spot, a constant current plateau in *I–V* curve was formed. The output current response of the rod in periodically changing pO_2 between 20% and 100% showed improved stability and reproducibility for $x=0.4$ compared to $x=0.2$. Improved oxygen absorption and desorption time was observed for $x=0.4$ compared to previously reported unsubstituted rod. On the other hand, for Mg-substituted rods the *I–V* behavior after formation of hot spot showed a negative slope. Faster absorption time of 3.0 s and desorption time of 6.9 s were observed for $y=0.4$ compared to $y=0.2$. The improved output current stability, reproducibility and response time is suggested to be due to changes in oxygen activation energy and increased hole concentration as a result of Ca^{2+}/Mg^{2+} substitutions. The Mg-substituted rods showed better performance compared to Ca-substituted rods possibly due to higher porosity and vacancy concentration.

Keywords: Eu123; Hot spot; Oxygen sensing; Ca/Mg substitution

1. Introduction

Ceramic gas sensors have played an important role in industries and have been continuously developed to improve sensing capabilities and performances. Some of the sensors currently used need to be activated by some form of external heating, for example, ZrO_2-type sensors which detects oxygen gas at operating temperature of above 400 °C [1,2]. Interestingly, a much simpler and self-heating oxygen sensor using $REBa_2Cu_3O_{7-\delta}$ (RE = Gd and Sm) polycrystalline ceramics based on the formation of oxygen sensitive hot spot upon application of external voltage have been reported [1,2].

The first discovery of the hot-spot based RE123 oxygen sensing element was made by Takata et al. [2] for Gd123 where the output current is sensitive to oxygen partial pressure concentration after the appearance of the hot spot at room temperature. The formation of the hot spot phenomena on $REBa_2Cu_3O_{7-\delta}$ rods is related to their positive temperature coefficient of resistivity (PTCR) characteristics [2–4] and oxygen nonstoichiometry. PTCR behavior in Gd123 materials have been reported by researches [3] whereby the oxygen content decreases with increasing temperature above 400 °C, resulting in steep increase in resistivity [5–8]. Under external voltage abnormal resistivity due to a microstructural defect point on the sensor rod is essential for formation of the hot spot triggered by a higher potential drop across the point caused by applied joule heating [2,9–11]. Oxygen is released from the heated point and resistivity of the point becomes higher than the rest of the rod. The temperature of the point increases with increasing applied voltage which in turn increases resistivity further until the point became a hot glowing spot. After appearance of the hot

*Corresponding author. Tel.: +603 5544 4613; fax: +603 5544 4562.
E-mail addresses: ahmad191@salam.uitm.edu.my, dr_ak_yahya@yahoo.com (A.K. Yahya).

0272-8842/$36.00 © 2012 Elsevier Ltd and Techna Group S.r.l. All rights reserved.
http://dx.doi.org/10.1016/j.ceramint.2012.04.088

spot, the output current decreases with increasing applied voltage before forming a constant-current plateau with further increase in voltage [2,3]. Oxygen sensing is based on the height of the plateau which shifts by an amount indicative of the concentration of oxygen absorbed by the hot spot [2,3].

In addition to the studies on single phased RE123 rods [2,3], secondary phases such as $BaAl_2O_4$ [4], CuO [12] and $BrZrO_3$ [13] had been carried out to improve oxygen response and repeatability of output current. However, these studies were based on longer sensor rods with length of around 30 mm. More recent studies on $REBa_2Cu_3O_{7-\delta}$ (RE=Er, Dy, Ho and Eu) [10,11,14–18] used shorter rods of around 12 mm length. The reports showed significant differences in current–voltage (*I–V*) characteristics and oxygen sensing characteristics compared to longer rods as a result of different heat distribution between its two ends. The output current after appearance of the hot spot for shorter rods, did not approach a constant value immediately but a plateau was formed more gradually with increasing applied voltage [10,11,14–18]. So, although shorter rods are more practical and cheaper for industrial use further study has to be carried out to produce *I–V* characteristics comparable to longer rods.

Quite recently, we have fabricated a 12 mm length $Eu_{0.9}Ca_{0.1}Ba_2Cu_3O_{7-\delta}$ rod and observed some improvement in its *I–V* characteristics upon appearance of the hot spot [18]. Thus in this paper, we further investigate oxygen sensing response of Eu123 short rods by studying in more detail the effects of Mg^{2+} and Ca^{2+} substitutions at Eu site. It is of particular interest to investigate the effects of substitutions of the divalent ions in place of trivalent Eu^{3+} as it was reported to induce structural changes in addition to an expected increase in intrinsic hole concentration in CuO_2 planes [19–25]. *I–V* characteristics of the rods were investigated in oxygen partial pressure, pO_2 from 10% to 100%. Results of output current response, oxygen absorption and desorption time behavior during alternating pO_2 between 20% and 100% are also reported.

2. Experimental

Bulk samples of $Eu_{1-x}Ca_xBa_2Cu_3O_{7-\delta}$ ($x=0.2$–0.5) and $Eu_{1-y}Mg_yBa_2Cu_3O_{7-\delta}$ ($y=0.2$–0.5) were synthesized by the conventional solid-state-reaction method. Appropriate amounts of high purity ($\geq 99.99\%$) Eu_2O_3, $BaCO_3$, CuO, MgO and CaO powders were weighed in stoichiometric ratio, mixed and ground. The ground powder was then calcined in a box furnace at 900 °C for 24 h with several intermittent grindings. The ground powder was then pressed into pellets and then sintered at 930 °C in a box furnace for 24 h followed by slow cooling to room temperature. The pellets were then cut into rods with each rod having dimensions of approximately 0.65 mm × 0.65 mm × 12 mm.

All the samples were subjected to Powder X-ray Diffraction (XRD) analyses using Rigaku model D/MAX 2000 PC with Cu-K_α radiation source to confirm the phase structures formed during the preparation process. The porosity, *P* of all the samples was computed using $P=(1-\rho/\rho_x)\times 100\%$ where ρ is the bulk density measured using the ordinary method and ρ_x is the X-ray density [26]. Oxygen deficiency range of $0<\delta<0.5$ was used to compute the uncertainty in the calculated porosity values. Microstructure was investigated using JEOL model JSM-6360LA scanning electron microscope (SEM).

Electrical characterization for *I–V* characteristics was measured using the standard four-point-probe method conducted under controlled in and out flow rate of partial pressure ranging from 10% to 100% of the oxygen-nitrogen gas mixture in a chamber. PTCR behavior of the rods was investigated by heating them in a box furnace from 30 °C to 900 °C at a rate of 7.5 °C min^{-1}. The temperature of the hot spot was measured by IMPAC non-contact pyrometer model IP 140 which can detect temperature for a hot spot size as small as 0.4 mm in the temperature range of 160 °C–1200 °C.

3. Result and discussion

Fig. 1 shows XRD patterns for $Eu_{1-x}Ca_xBa_2Cu_3O_{7-\delta}$ ($x=0$, 0.2,0.4) and $Eu_{1-y}Mg_yBa_2Cu_3O_{7-\delta}$ ($y=0$,0.2,0.4). The XRD analysis confirmed that all samples consist of single phased 123 orthorhombic structures with space group *Pmmm* with some small amount of impurity unidentified. From this figure, the Mg-substituted intensity was smaller compared to the Ca-substituted samples. This showed that the crystallinity of the Ca-substituted was higher than the Mg-substituted samples.

The current–voltage (*I–V*) characteristics of the $Eu_{1-x}Ca_xBa_2Cu_3O_{7-\delta}$ and $Eu_{1-y}Mg_yBa_2Cu_3O_{7-\delta}$ rods before and

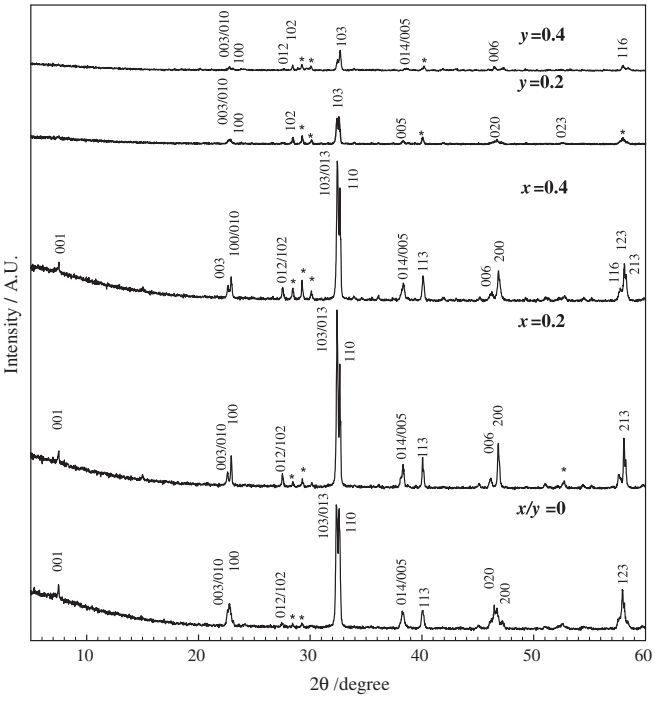

Fig. 1. XRD patterns for $Eu_{1-x}Ca_xBa_2Cu_3O_{7-\delta}$ ($x=0$, 0.2, 0.4) and $Eu_{1-y}Mg_yBa_2Cu_3O_{7-\delta}$ ($y=0$, 0.2, 0.4) samples. The (*) sign are the impurity phases.

after appearance of hot spots at different oxygen partial pressure, pO_2 from 10% to 100% are shown in Fig. 2. The *I–V* curves for all samples show the output current for each pO_2 value increases linearly with applied dc voltage until the appearance of the visible hot spot as indicated by the arrows. Previous studies of the *I–V* curves behavior for Ca-free ceramic rods [18], showed decreasing output current after the appearance of the hot spot with increasing applied voltage. However, in the present study we found that the output current for $x=0.2$ continued to increase after the appearance of the hot spot. At a certain applied voltage value, the current then starts to become constant. But for the $x=0.4$ sample, a stable current forms almost immediately after appearance of the hot spot. Similar to the Ca-substituted rods, the output current for Mg-substituted samples for each pO_2 value increases linearly with applied dc voltage until the appearance of a visible hot spot. However, unlike the Ca-substituted samples, the output current for the Mg-substituted samples decreases with further increase in applied voltage. Furthermore, we found that Mg substitution has lowered the output current further than the Ca-substituted samples. As the temperature of the hot spot increases with increasing applied voltage [2,10], to avoid breakage due to melting the highest voltage applied on each rod sample was limited to a certain value. For all x and y values, the output current of the respective ceramic rods especially after the appearance of the hot spot clearly and strongly depended on pO_2 concentrations.

Fig. 3 shows SEM images of the internal section of the rod after hot spot formation for $Eu_{1-x}Ca_xBa_2Cu_3O_{7-\delta}$ ($x=0.2$, 0.4) and $Eu_{1-y}Mg_yBa_2Cu_3O_{7-\delta}$ ($y=0.2$, 0.4). All rods showed irregular grains along with some level of porosity. The microstructure of $x=0.2$ and 0.4 rods showed irregular grains with average grain size of 8 μm and 6 μm, respectively, while the rod with $y=0.4$ showed slightly smaller irregular grains with average grain size of 4 μm compared to the $y=0.2$ rod whose average grain size was 6 μm. The calculated percentages of porosity values for different Ca and Mg concentrations are shown in Table 1. Mg substituted rods clearly showed larger porosity values of 17% ($y=0.2$) and 22% ($y=0.4$) compared to Ca substituted rods which only showed 10%–11% porosity.

Fig. 4 shows the output current response for repeated switching of pO_2 concentrations between 20% and 100% for a period of 7 min each for $Eu_{1-x}Ca_xBa_2Cu_3O_{7-\delta}$ ($x=0.2$, 0.4) and $Eu_{1-y}Mg_yBa_2Cu_3O_{7-\delta}$ ($y=0.2$, 0.4) rods in the presence of a hot spot at different operating voltages. The switch to a higher or lower oxygen partial pressure leads to an increase or decrease of the output current, respectively. It is observed that the response time of the $x=0.4$ rod for the output current to change between the switching of the pO_2 concentrations is much faster than

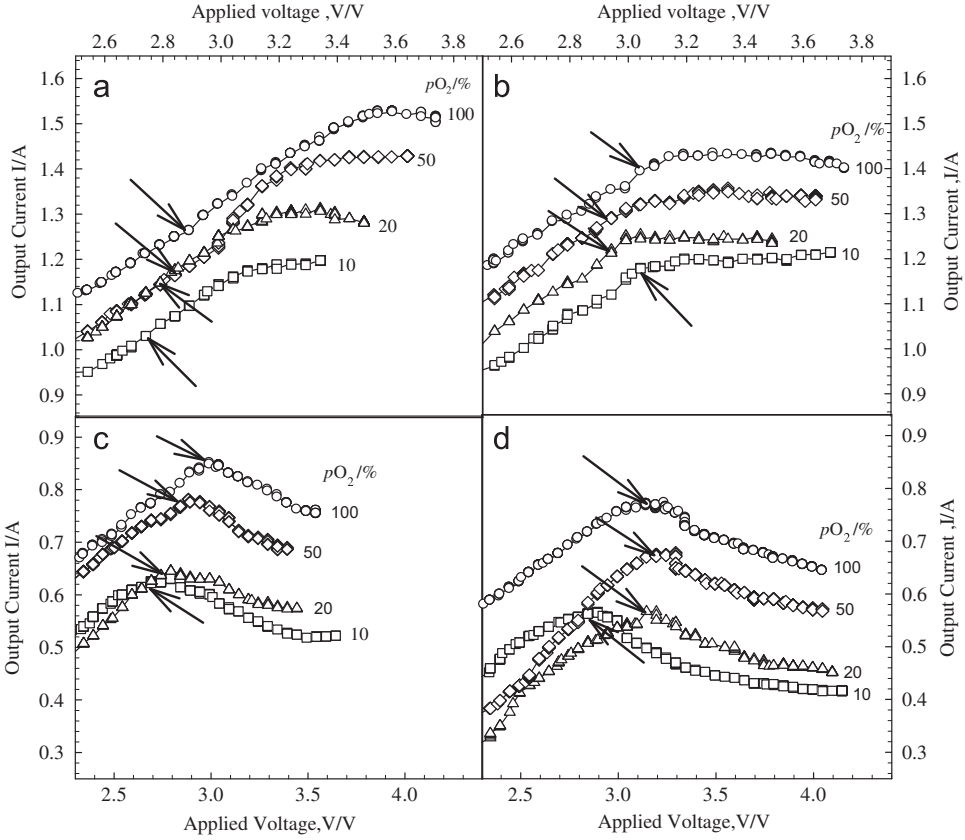

Fig. 2. Output current versus applied voltage for $Eu_{1-x}Ca_xBa_2Cu_3O_{7-\delta}$ and $Eu_{1-y}Mg_yBa_2Cu_3O_{7-\delta}$ for (a) $x=0.2$, (b) $x=0.4$, (c) $y=0.2$ and (d) $y=0.4$ at different pO_2. The arrows indicate appearance point of visible hot-spots.

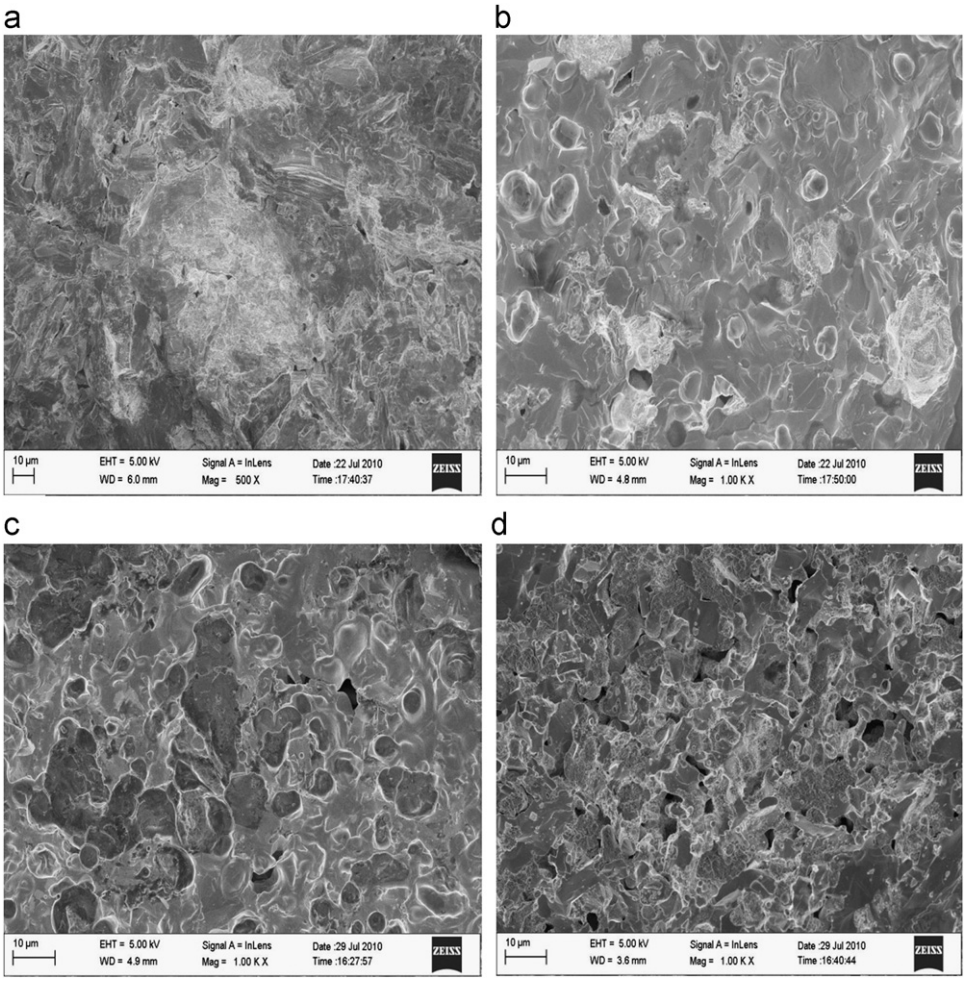

Fig. 3. SEM image of the internal section of the rod after hot spot formation for $Eu_{1-x}Ca_xBa_2Cu_3O_{7-\delta}$ for (a) $x=0.2$, (b) $x=0.4$ and $Eu_{1-y}Mg_yBa_2Cu_3O_{7-\delta}$, (c) $y=0.2$ and (d) $y=0.4$ rods.

Table 1
The density, porosity, time response of oxygen absorption and desorption of the samples $(Eu_{1-x}Ca_x)Ba_2Cu_3O_{7-\delta}$ ($x=0$, 0.2, 0.4) and $(Eu_{1-y}Mg_y)Ba_2Cu_3O_{7-\delta}$ ($y=0$, 0.2, 0.4).

Sample/concentration (x,y)	Density, ρ (g/cm^3)	Porosity, P (%)	Absorption time, t_{abs} (s)	Desorption time, t_{des} (s)
(0,0)	5.8 ± 0.2	14 ± 1	142.7 [Ref. 18]	145.0 [Ref. 18]
(0.2,0)	5.9 ± 0.2	10 ± 1	–	–
(0.4,0)	5.7 ± 0.2	11 ± 1	64.5	93.1
(0,0.2)	5.7 ± 0.3	17 ± 1	58.0	78.1
(0,0.4)	5.2 ± 0.2	22 ± 1	3.0	6.9

for the $x=0.2$ rod which has resulted in an almost abrupt change of the output current when the switch was made. At the same operating voltage of 3.65 V (Figs. 4(c) and (d)), the $y=0.4$ rod shows instability in the output current as compared to the $y=0.2$ sample. However, at a higher operating voltage of 3.9 V, the output current for the $y=0.4$ rod attained better stability.

Since the sensor current clearly depends on pO_2, the output current response time could be linked to the rate of absorption and desorption of oxygen in the presence of a hot spot. In this work we defined absorption time, t_{abs} and desorption time, t_{des} as the time for output current to increase to saturation level and the time for output current from saturation level to decrease to initial level, respectively, as shown in Fig. 5.

The oxygen absorption time, t_{abs} and oxygen desorption time, t_{des} for $Eu_{1-x}Ca_xBa_2Cu_3O_{7-\delta}$ ($x=0.2$ and $x=0.4$) and $Eu_{1-y}Mg_yBa_2Cu_3O_{7-\delta}$ ($y=0.2$ and $y=0.4$) are shown

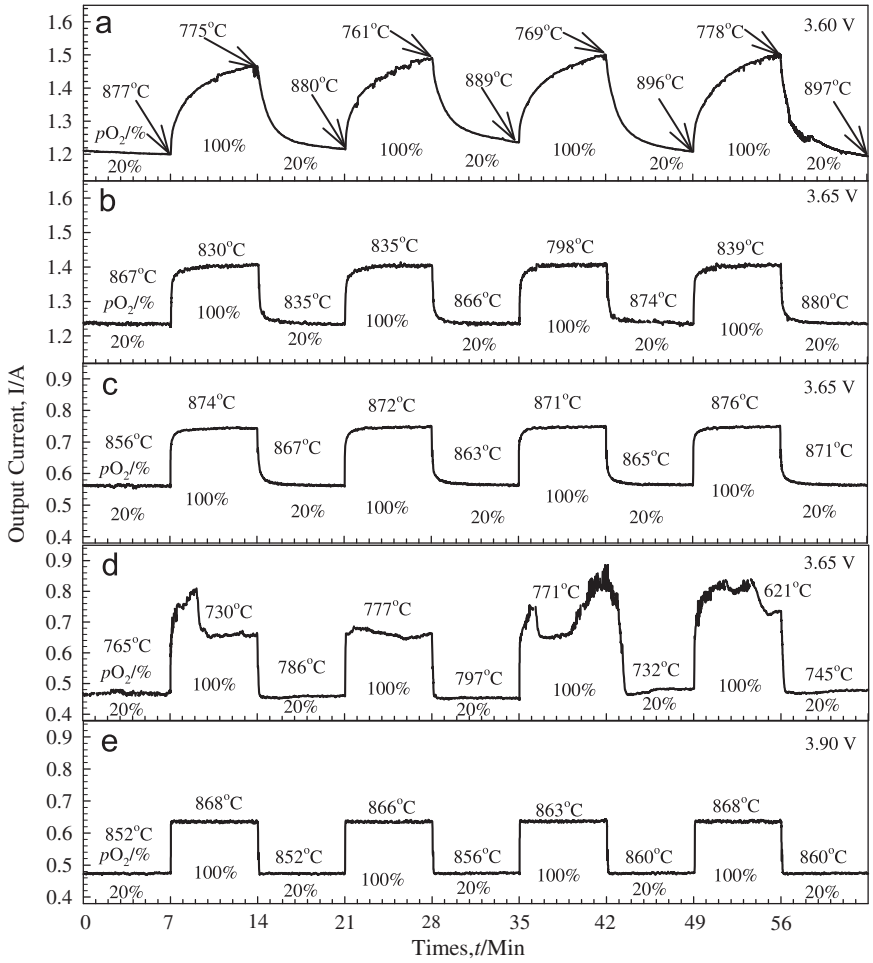

Fig. 4. Response of output current of $Eu_{1-x}Ca_xBa_2Cu_3O_{7-\delta}$ rods for (a) $x=0.2$, (b) $x=0.4$ rods operating at 3.6 V and $Eu_{1-y}Mg_yBa_2Cu_3O_{7-\delta}$, (c) $y=0.2$ rod operating at 3.65 V, (d) $y=0.4$ rod operating at 3.65 V and (e) $y=0.4$ rod operating at 3.90 V with pO_2 changing periodically between 20% and 100%.

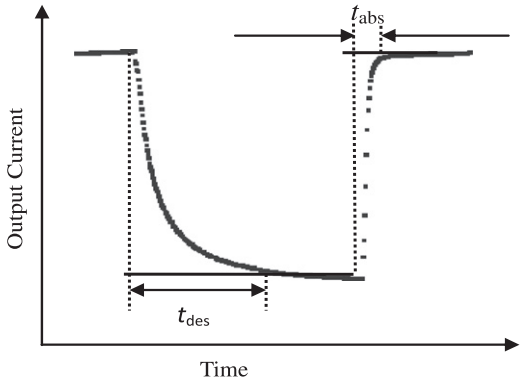

Fig. 5. Diagram showing desorption time, t_{des} and absorption time, t_{abs} for decrease and increase in output current respectively.

in Table 1. Among the Ca-substituted samples, the $x=0.4$ rod produces t_{abs} and t_{des} of 64.5 s and 93.1 s, respectively. Interestingly enough, the Mg substitution of $y=0.4$ have produced an even shorter t_{abs} and t_{des} than the Ca-substituted $x=0.4$ rod, showing an improved time of 3.0 s and 6.9 s, respectively. Even though the t_{abs} and t_{des} for $x=0.2$ could not be calculated as current saturation level was not achieved within the seven minute limit, the results of the other substitutions indicate that substitution at the Eu-site has improved oxygen desorption and absorption with a smaller time response when compared to previously reported unsubstituted $EuBa_2Cu_3O_{7-\delta}$ rod [18]. The substitutions of divalent Ca^{2+}/Mg^{2+} for trivalent Eu^{3+} may have caused physical changes in the materials which lead to the differences in oxygen response.

Previous studies on Y123 system has suggested that increasing concentration of Ca^{2+} substitution at Y^{3+} site affects oxygen bonding to neighboring atoms in the Y123 structure. The rapid increase in Ba–O(1) bond length due to displacement of Ba ions away from the Cu–O chain and towards the CuO_2 plane causes oxygen to be removed more easily at elevated temperatures [25]. The difference in oxygen sensing behavior between the $(Eu,Ca)Ba_2Cu_3O_{7-\delta}$ and $(Eu,Mg)Ba_2Cu_3O_{7-\delta}$ series (Fig. 2) may be due to changes in oxygen activation energy which leads to easier removal and intake of oxygen caused as a result of the substitutions. On the other hand, the sensing behavior may also be influenced by the increase in intrinsic hole as a

result of divalent Ca^{2+}/Mg^{2+} substitution for trivalent Eu^{3+}. The higher hole concentration is expected to reduce oxygen intake in order to maintain charge neutrality and this could be the reason for the lower sensitivity of the rod to pO_2. This could be clearly seen for the Ca-substituted series which displayed flatter and more closely spaced current plateau for $x=0.4$ compared to $x=0.2$. In addition to the above, other factors such as differences in crystallinity (Fig. 1) and porosity (Table 1) may also influence the oxygen sensing performance. The lower crystallinity for Mg substituted rods suggest existence of more defects or vacancies [27–29] compared to Ca-substituted rods while its higher porosity facilitates oxygen diffusion in the hot spot area [30,31].

Besides the output current response to pO_2, the hot spot temperature for both $x=0.2$ and $x=0.4$ samples were observed to drop to lower temperature at higher oxygen concentration as shown in Fig. 4(a) and (b). The decrease in hot spot temperature with increasing pO_2 may be due to insufficient joule heating [10] which caused slower oxygen absorption and oxygen desorption as in Fig. 4(a). In contrast, the hot spot temperatures of $Eu_{1-y}Mg_yBa_2Cu_3O_{7-\delta}$ rods in Figs. 4(c) and (e) were observed to be higher at 100% pO_2 concentration than at 20% pO_2 concentration. However, the hot spot temperature of the $y=0.4$ rod operating at 3.65 V (Fig. 4(d)) was observed to have the similar behavior as the Ca-substituted samples. While insufficient joule heating causes slower oxygen absorption and oxygen desorption for the Ca-substituted samples, insufficient joule heating in the $y=0.4$ rod operating at 3.65 V causes instability of the output current [10]. The higher hot spot temperature for Mg substituted rods and their faster absorption and desorption times are suggested to be due to their higher porosity and vacancy concentration which enhanced oxygen diffusion in the hot spot area and sustained hot spot heating.

Fig. 6 shows the change of resistivity of the $Eu_{1-x}Ca_xBa_2Cu_3O_{7-\delta}$ ($x=0$, 0.2, 0.4) and $Eu_{1-y}Mg_yBa_2Cu_3O_{7-\delta}$ ($y=0$, 0.2, 0.4) rods with temperature. The Ca and Mg-free sample showed PTCR characteristics above 600 °C while all the substituted samples generally showed PTCR characteristics above 400 °C. However, the Mg-substituted samples show a steeper increase in resistivity over 400 °C as compared to the Ca-substituted samples. Previous reports on RE123 system showed if the temperature of the sample is increased above 400 °C, oxygen is lost from the structure [5] and carrier density decreases, which resulted in an increase in the resistivity [6–8].

The constant output current plateau formation in Fig. 2(a) and (b) after the appearance of the hot spot for the Ca-substituted $x=0.2$ and $x=0.4$ rods may be related to the PTCR behavior in Fig. 6. We observed that the hot spot appeared around 600 °C for Ca-substituted $x=0.2$ and $x=0.4$ samples but the increase in resistivity over 600 °C (Fig. 6) is very small. As a result, the almost constant output current formed after the appearance of the hot spot with increasing applied voltage for Ca-substituted samples could be due to the slow increase

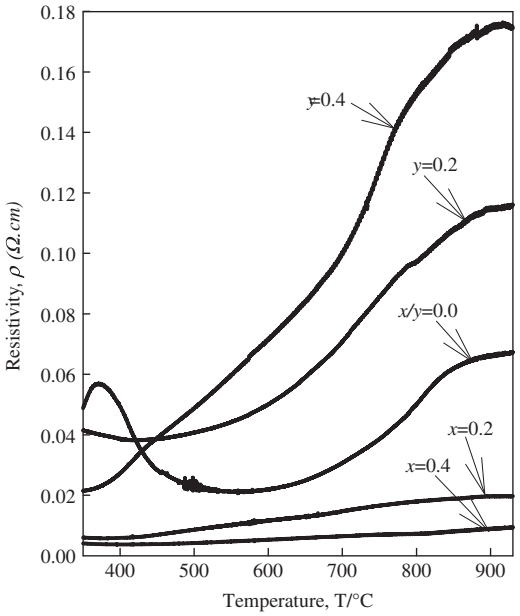

Fig. 6. Plot of resistivity versus temperature for $Eu_{1-x}Ca_xBa_2Cu_3O_{7-\delta}$ ($x=0$, 0.2, 0.4) and $Eu_{1-y}Mg_yBa_2Cu_3O_{7-\delta}$ ($y=0$, 0.2, 0.4) ceramics.

in resistivity of the hot spot area. On the other hand, for Mg-substituted $y=0.2$ and 0.4 rods (Fig. 6), the resistivity increases steeply with temperature compared to Ca-substituted samples above the hot spot temperature (approximately around 600 °C) causing the output current after appearance of the hot spot to decrease with increasing applied voltage. This observation is in agreement with *I–V* behavior reported in previous studies on hot-spot based Er123 [10], Gd123 and Sm123 rods [2,3].

The difference in PTCR behavior (Fig. 6) between $(Eu,Ca)Ba_2Cu_3O_{7-\delta}$ and $(Eu,Mg)Ba_2Cu_3O_{7-\delta}$ rods is suggested to be due to the differences in oxygen loss with increasing temperature as a result of the substitutions. As temperature increases beyond 420 °C, the resistivities of the $y=0.2$ and $y=0.4$ rods showed much steeper increase compared to the $x=0.2$ and $x=0.4$ rods. The resistivity behavior indicates larger loss of oxygen content for the Mg^{2+} substituted rods while the Ca^{2+} substitution may have caused lower oxygen loss. Such behavior may be related to differences in oxygen activation energy between Mg^{2+} and Ca^{2+} substituted rods as mentioned earlier. We propose that Mg^{2+} substitution with $y=0.4$ resulted in a larger reduction in oxygen activation energy compared to Ca^{2+} substitution of $x=0.4$. Since Ca and Mg are both divalent, the effect may be induced by the larger difference in ionic radius of Ca^{2+} (1.03 Å) and Mg^{2+} (0.72 Å) when substituted at the Eu-site (1.02 Å) [32]. Substituting Mg^{2+} which has a smaller ionic radius than Eu^{3+} would probably cause a larger change in internal cell pressure compared to Ca^{2+} that has almost similar ionic radius as Eu^{3+} and this would lead to differences in activation energies.

The oxygen sensing behavior for Ca-substituted and Mg-substituted rods are presented by the plot of output current versus pO_2 concentrations in Fig. 7. A steeper slope

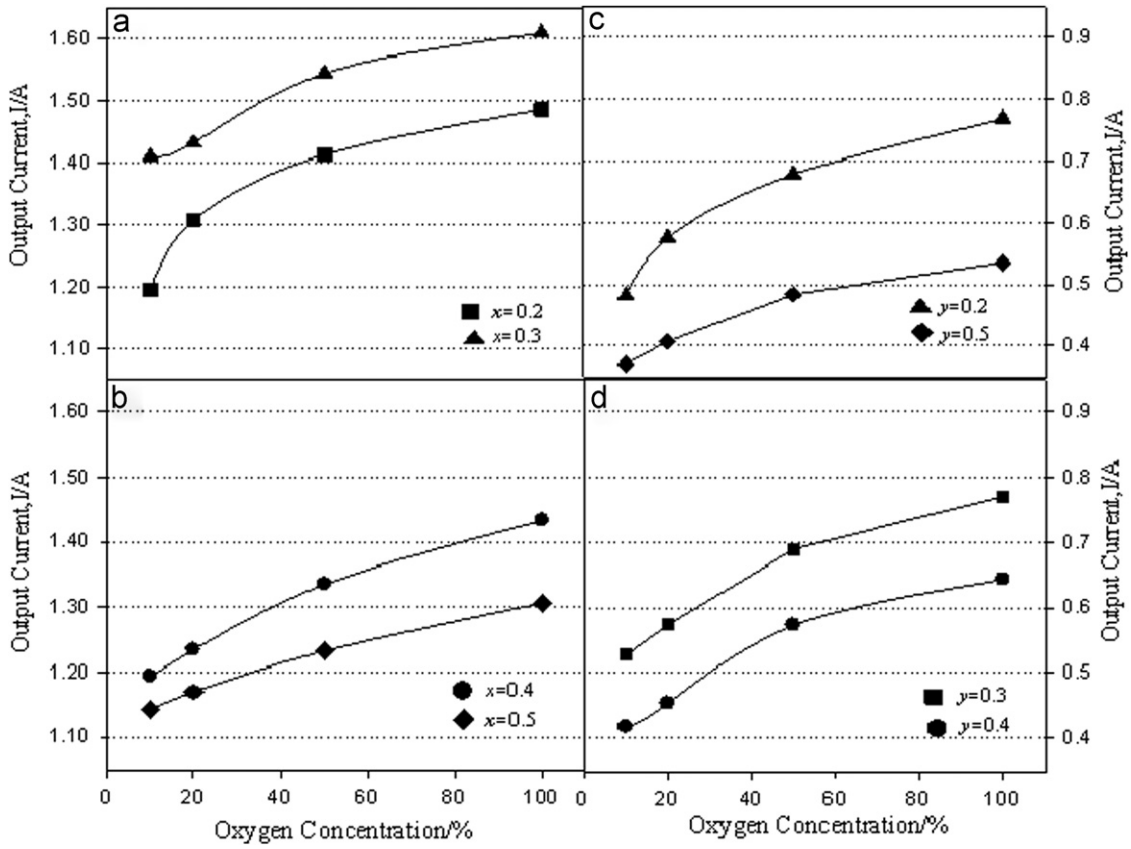

Fig. 7. Output current versus pO_2 for (a) $Eu_{1-x}Ca_xBa_2Cu_3O_{7-\delta}$ (x=0.2, 0.3), (b) $Eu_{1-x}Ca_xBa_2Cu_3O_{7-\delta}$ (x=0.4, 0.5), (c) $Eu_{1-y}Mg_yBa_2Cu_3O_{7-\delta}$ (y=0.2, 0.5) and (d) $Eu_{1-y}Mg_yBa_2Cu_3O_{7-\delta}$ (y=0.3, 0.4) sensor rods.

would indicate greater sensitiveness to the change in oxygen level. The slopes for the x=0.2 and y=0.2 rods indicate the highest sensitiveness to oxygen below 20% pO_2 concentration. Higher sensitiveness to oxygen below 20% pO_2 concentration was also similarly reported in previous report on un-substituted Eu123 rods [18]. However, the difference in oxygen sensitivity between low and high pO_2 regions in Fig. 7 (for x=0.2 and y=0.2) and un-substituted Eu123 rod [18] may originate from structural differences triggered by the difference in hot spot temperatures. Previous report on Sm123 sensor rod has shown that increasing pO_2 causes the hot spot temperature to increase. While a detailed study on Er123 sensor rod [10] suggests that the Er123 structure undergoes a change from orthorhombic to tetragonal around 700 °C. As such, it is suggested that the lower sensitiveness to oxygen above 50% pO_2 concentration for x/y=0, x=0.2 and y=0.2 rods may be related to similar structural change which occur at hot spot temperatures above 700 °C.

Takata et al. [2] suggest that the oxygen sensing property of RE123 hot spot can be explained by the absorption of oxygen gas which then dissociates into oxide ions and holes. The overall reaction during the absorption and desorption of oxygen gas could be expressed as

$$O_2 \rightleftarrows 2O_i^{2-} + 4h^+ \quad (1)$$

where O_i^{2-} is an oxide ion and h^+ is a hole. The absorption of oxygen produces significant change in conductivity which is translated as the magnitude of the output current. The change in magnitude of the output current indicates the presence of different levels of oxygen concentration. Application of the mass action law on Eq. (1) shows that the conductivity, σ is related to oxygen concentration by

$$\sigma \propto pO_2^{1/6} \quad (2)$$

The relation of the log of output current and log of pO_2 concentrations in Fig. 8 shows linear curves for Ca and Mg-substituted rods from 10% to 100% pO_2. Interestingly the slope in Fig. 8(c) and (d) for Mg-substituted rod series is very close to the ideal value of 1/6 for ideal case of materials with excess oxygen as given in Eq. (2). The closeness of the calculated slopes to the mass action law may very well explain the behavior of the output current in Fig. 7(c) and (d). However, our study showed that substitution of Ca with x=0.2–0.5 caused slight deviation from the ideal value of 1/6 as seen in Fig. 8(a) and (b). The reason for deviation from the ideal value of 1/6 of $Eu_{1-x}Ca_xBa_2Cu_3O_{7-\delta}$ (x=0.2–0.5) rod is probably due to the insufficient joule heating. The temperature of the hot spot decreases even with increasing pO_2. This will result in slower oxygen diffusion which causes charge carriers formed from dissociations of absorbed oxygen at the hot

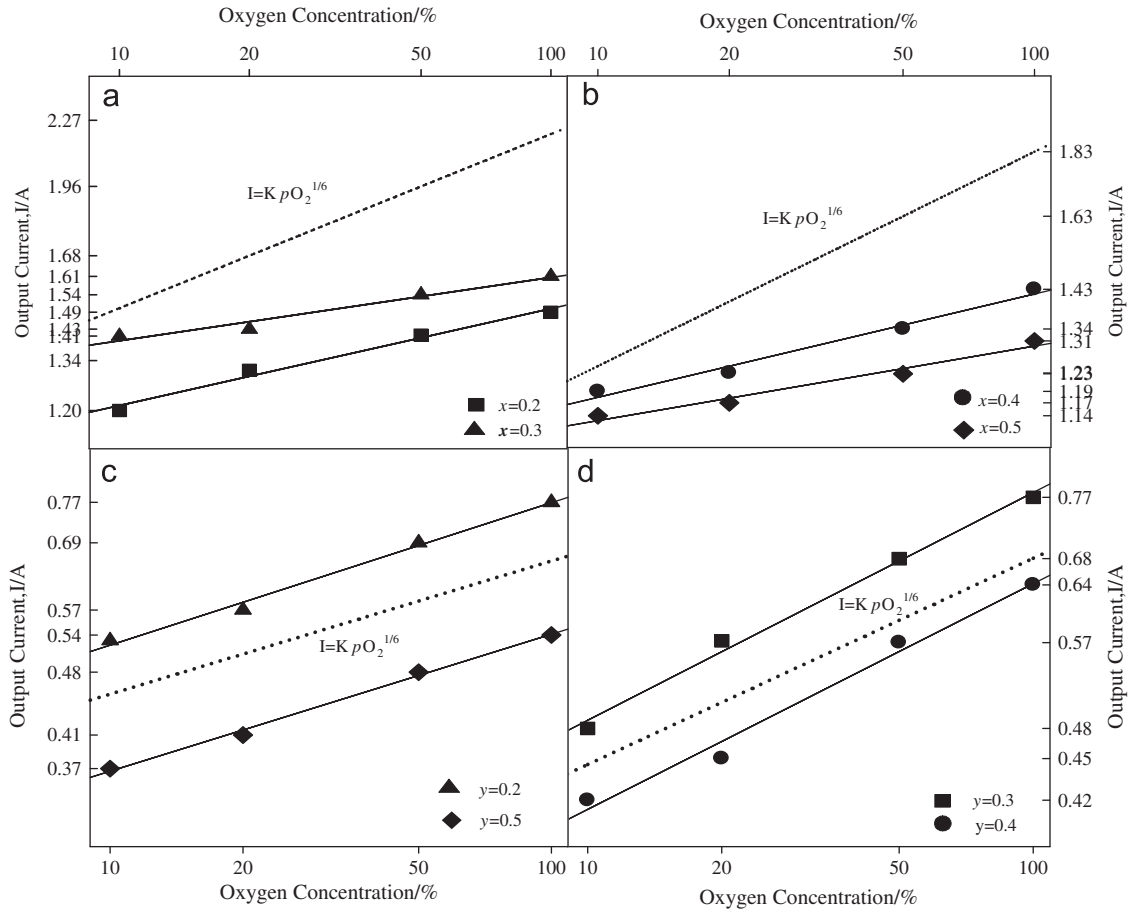

Fig. 8. The relation between log of output current and log of pO_2 concentration for (a) $Eu_{1-x}Ca_xBa_2Cu_3O_{7-\delta}$ ($x=0.2$, 0.3), (b) $Eu_{1-x}Ca_xBa_2Cu_3O_{7-\delta}$ ($x=0.4$, 0.5), (c) $Eu_{1-y}Mg_yBa_2Cu_3O_{7-\delta}$ ($y=0.2$, 0.5) and (d) $Eu_{1-y}Mg_yBa_2Cu_3O_{7-\delta}$ ($y=0.3$, 0.4) sensor rods. The dotted line is based on $I=KpO_2^{1/6}$ and drawn as a guide to the eye.

spot to become no longer dominant and conductivity is suggested to depend on intrinsic carriers.

4. Conclusion

The *I–V* behavior of (Eu,Ca)$Ba_2Cu_3O_{7-\delta}$ rods after appearance of a hot spot showed stable output current which formed a plateau upon increase in voltage under different pO_2. However, (Eu,Mg)$Ba_2Cu_3O_{7-\delta}$ rods showed decreasing output current before approaching a constant value with increasing voltage under the same pO_2 conditions. Higher Ca^{2+}/Mg^{2+} substitution showed improvement in output current stability, reproducibility and response time compared to lower doped rods. The higher doping was suggested to cause changes in activation energy and increase in hole concentration which is responsible for the difference in oxygen response. Overall Mg substituted rods showed better performance with the fastest oxygen absorption and desorption times of 3.0 s and 6.9 s respectively, recorded for the $y=0.4$ rod. The better sensing performance was suggested to be due to the higher porosity and vacancy concentration which facilitates oxygen diffusion in the hot spot area.

References

[1] Usui Toshio, Asada Akiyoshi, Nakazawa Mitsuhiro, Osanai Hiroshi, Gas polarographic oxygen sensor using an oxygen/zirconia electrolyte, Journal of the Electrochemical Society 136 (2) (1989) 534–542.
[2] M. Takata, Y. Noguchi, Y. Kurihara, T. Okamoto, B. Huybrechts, Novel oxygen sensor using hot spot on ceramic rod, Bulletin of Materials Science 22 (3) (1999) 593–600.
[3] T. Okamoto, Y. Ibaraki, M. Takata, Hot spot in $LnBa_2Cu_3O_{7-\delta}$ ceramic and its applications, Journal of the Ceramic Society of Japan 112 (5) (2004) S582–S587.
[4] T. Okamoto, M. Takata, Development of functional devices using hot spot in $GdBa_2Cu_3O_{7-\delta}$-based composite ceramics, Ceramics International 30 (7) (2004) 1569–1574.
[5] K. Kishio, J. Shimoyama, T. Hasegawa, K. Kitazawa, K. Fueki, Determination of oxygen non-stoichiometry in high-Tc superconductor $Ba_2YCu_3O_{7-\delta}$, Japanese Journal of Applied Physics 26 (1987) L1228.
[6] V.A.M. Brabers, W.J.M. de Jonge, L.A. Bosch, C.v.d. Steen, A.M.W. de Groote, A.A. Verheyen, C.W.H.M. Vennix, Annealing experiments on and high-temperature behaviour of the superconductor $YBa_2Cu_3O_x$, Materials Research Bulletin 23 (1988) 197.
[7] A.T. Fiory, M. Gurvitch, R.J. Cava, G.P. Espinosa, Effect of oxygen desorption on electrical transport in $YBa_2Cu_3O_{7-\delta}$, Physical Review B 36 (1987).
[8] T.K. Chaki, M. Rubinstein, Normal-state resistivity of the high-Tc compound $Y_1Ba_2Cu_3O_{7-\delta}$, Physical Review B 36 (1987) 7259.

[9] T. Okamoto, B. Huybrechts, M. Takata, Electric field sensitive moving hot spot in $GdBa_2Cu_3O_{7-\delta}$ ceramics, Japanese Journal of Applied Physics 33 (1994) L1212–L1214.
[10] M. Hassan, A.K. Yahya, Influence of hot-spot temperature on oxygen sensing response behavior of Er123 ceramic rods with hot spot, Journal of Alloys and Compounds 499 (2010) 206–211.
[11] M. Hassan, A.K. Yahya, T. Okamoto, Effect of $BaAl_2O_4$ addition on power consumption and oxygen sensing response of Er123 ceramic rods utilizing hot-spot phenomenon, Sains Malaysiana 40 (1) (2011) 27–33.
[12] K. Iihama, Y. Kuroki, T. Okamoto, M. Takata, Characteristics of hot spot oxygen sensor using $GdBa_2Cu_3O_{7-\delta}$-CuO composite ceramics, Current Applied Physics 9 (2009) S167–S169.
[13] Y. Tsutai, T. Okamoto, A. Kawamoto, M. Takata, Hot spot $GdBa_2Cu_3O_{7-\delta}$-$BaZrO_3$ composite ceramics, Journal of the Ceramic Society of Japan 112 (5) (2004) S599–S601.
[14] M. Hassan, A.K. Yahya, K.H. Ku Hamid, Z. Awang, Fabrication and characterization of oxygen sensing properties of Dy123 sensor utilizing hot spot phenomenon, AIP Conference Proceedings 1017 (2008) 295–299.
[15] M. Hassan, A.K. Yahya, Oxygen response of hot spot on $DyBa_2Cu_3O_{7-x}$ ceramic sensors fabricated under different heat treatments, Material Research Innovations 13 (3) (2009) 357–360 (4).
[16] L.H. Idrus, A.K. Yahya, Resistance-based ceramic Ho123 ionic conductor for oxygen gas sensing, AIP Conference Proceedings 1150 (2009) 219–222.
[17] L.H. Idrus, T. Okamoto, A.K. Yahya, Effect of ionic size on oxygen sensing properties of Sr substituted Ho123 ceramic rods utilizing hot spot phenomenon, Materials Research Innovations 15 (2) (2011) s144–s147.
[18] S.A. Yaacob, A.K. Yahya, M. Hassan, R. Hasham, Influence of intrinsic hole concentration on oxygen sensing properties of hot-spot based $Eu_{1-x}Ca_xBa_2Cu_3O_{7-\delta}$ ceramics, AIP Conference Proceedings 1250 (2010) 313–316.
[19] Rajiv Givi, V.P.S. Awana, H.K. Singh, R.S. Tiwari, O.N. Srivastava, A. Gupta, B.V Kumaraswamy., H. Kishan, Effect of Ca doping for Y on structural/microstructural and superconducting properties of $YBa_2Cu_3O_{7-\delta}$, Physica C 419 (2005) 101–108.
[20] P. Starowicsz, J. Sokolowski, M. Balanda, A. Szytula, The effect of calcium substitution in deoxygenated $R_{1-x}Ca_xBa_2Cu_3O_{6.1}$ system (R=Y,Eu): appearance of superconductivity, insulator to metal transition, Physica C 363 (2001) 80–90.
[21] A. Szytula, P. Starowicsz, B. Penc, The influence of doping on the electronic structure of $R_{1-x}Ca_xBa_2Cu_3O_{6+d}$ (R=Y,Eu) and $(La_{0.7}Ca_{0.3})_{1-x}Mn_{1+x}O_3$, Physica C 387 (2003) 272–276.
[22] Hajime Kenji Hatada, Shimizu, Structural and superconducting properties of $R_{1-x}Ca_xBa_2Cu_3O_{6+\delta}$ (R=Y Er, Gd, Eu; $0<\delta<1$), Physica C 304 (2001) 89–95.
[23] G. Botter, J. Mesot, P. Fischer, A. Furrer, Ca substitution in $RBa_2Cu_3O_{7-\delta}$ (R=Y,Er; $\delta<0.15$): the influence on structure and superconductivity, Physica B 234–236 (1997) 843–845.
[24] Song Hongzhang, Huang Miaomiao, Yang Delin, Hu Xing, Li Yongxiang, Oxygen permeability of perovskite-type $Y_{1-x}M_xBa_2Cu_3O_{7-\delta}$ (M=La,Ca) membranes, Materials Science & Engineering B 137 (2007) 284–288.
[25] Dong Han Ha, Hyung Sik Min, Kyu Won Lee, Effects of cation substitution on the oxygen loss in YBCO superconductors, Journal of Korean Physical Society 39 (2001) 1041–1045.
[26] Y.S. Reddy, V. Prashanth Kumar, M.V. Ramana Reddy, P. Veerasomaniah, C. Vishnuvardhan Reddy, Elastic moduli of $Pr_{1-x}Sr_xMnO_3$ at 300 K, Invertis Journal of Science & Technology 1 (3) (2007) 236–240.
[27] L.D. Marks, J.P. Zhang, S.-J. Hwu, K.R. Poeppelmeier, Order-disorder in $YBa_2Cu_3O_7$, Journal of Solid State Chemistry 69 (1987) 189–195.
[28] G. Van Tendeloo, S. Amelinckx, Defect structure of superconducting $YBa_2Cu_3O_{7-\delta}$, Journal of Electron Microscopy Technique 8 (1988) 285–295.
[29] C.G.S. Pillai, Thermal conductivity of $YBa_2Cu_3O_{7-\delta}$ from ambient to 1150 K, Solid State Communications 80 (4) (1991) 277–280.
[30] R.Ravender Reddy, Prakash Om, P.Venugopal Reddy, The effect of Porosity on elastic moduli of $YBa_2Cu_3O_{7-\delta}$ high Tc superconductors, Applied Superconductivity 3 (4) (1995) 215–222.
[31] R.M. do Nascimento, J.M.A. Gimenez, C.R. Grandini, A.G. Cunha, Oxygen mobility in $SmBa_2Cu_3O_{7-\delta}$ measured by elastic spectroscopy, Material Science and Engineering A 442 (2006) 79–81.
[32] M. Buchgeister, P. Herzog, S.M. Hosseini, K. Kopitzki, D. Wagener, Oxygen evolution from $ABa_2Cu_3O_{7-\delta}$ high-Tc superconductors with A=Yb, Er, Y, Gd, Eu Sm, Nd and La, Physica C 178 (1–3) (1991) 105–109.